Denoising for Low-dose Computed Tomography

Zhiling Zou, and Zhongyuan Zhang

Abstract—Computed Tomography is a popular medical image examination tool. Low-dose computed chromography (LDCT) has been introduced recently to control the radiation side effects on patients. However, LDCT scans often have low contrast and high noise levels, which limits the adoption rate of LDCT. In this work, five denoising methods are implemented and evaluated on their ability to improve image quality at different noise levels in quantitative measures: Peak signal-to-noise ratio (PSNR) and mean square error (MSE) and qualitative measure: visualization. Among the methods, ADMM conserves most anatomical details, while convolutional Autoencoder provides the most consistent denoising performance. Denoised LDCT images can be used as good references in future clinical diagnoses.

Index Terms—Image Denoising, Computed Tomogrpahy

1 Introduction

Computed Tomography (CT) is a widely used medical screening tool. This X-ray technology produces high-quality cross-sectional images and can be used to show various anatomical structures in great detail, including bones, muscles, organs, and blood vessels. In clinical settings, CT scans are commonly used in disease diagnosis and many surgical interventions [1]. One major concern about using CT is its high radiation exposure. When a series of scans are needed to monitor some disease progression or recovery continuously, the cumulative radiation toxicity of CT scans will cause radiation syndrome and increase the risk of developing fatal cancer [2].

To address the toxicity problem of Full-dose CT (FDCT) scans, clinicians started to reduce the radiation dose to half or a quarter of the regular dose [3]. This is named Low-dose CT scans (LDCT). Although LDCT lowers radiation exposure significantly, it is not a perfect solution. LDCT does not provide image output of similar quality as FDCT in many cases. Lowering the dose would unavoidably increase the data noise and decrease the image contrast, affecting clinicians' disease diagnosis decisions [4].

In this project, we reviewed a set of computational image-denoising algorithms to improve the LDCT image quality to support future clinical research and patient usage.

2 Related Work

Image denoising has been widely investigated in the past. Computational denoisers are mainly classified in two categories: filter-based methods and model-based methods.

Some of the early works utilize linear and nonlinear filters to remove noise in the spatial domain. Examples include mean filtering, Wiener filtering and bilateral filtering. Spatial filtering can eliminate noise considerably. However, image blurring is often observed in their results [5]. In addition to spatial domain filtering, transformation techniques have also been developed to explore noise in different domains. Examples include Fourier transform, wavelet transform, and cosine transform [6].

Non-quadratic regularization models are later studied to address the blurring issue. Total variation-based regularization models and non-local regularization models have shown promising results, and great success has been achieved by a combined model in [7]. The limitation of this method is the loss of structural information. Thus, visual image quality is still not ideal.

To further improve denoising performance, model-based optimization methods and convolutional neural network (CNN) based methods are proposed. Model-based optimization involves iterative inference optimization upon the image prior. Popular methods include the Adam and Alternating Direction Method of Multipliers (ADMM). Long-running time is the major concern when using model-based methods on large datasets.

With the advanced development in computing hardware and software, deep learning models recently draw a lot of attention in image processing tasks, including image denoising [8]. CNN based methods minimize a loss function through training on a set of degraded-truth image pairs. Different neural network structures are designed for different purposes. Neural networks-based denoisers can achieve competitive denoising performance and acceptable running time.

3 Methods and Evaluations

In this section, we will first discuss five denoising methods: one linear estimation method, two neural network-based methods and two ADMM-based methods. Then, the data set and data pre-processing steps will be described. Lastly, we will represent the experimental setup used to evaluate the denoising performances.

3.1 Wiener Filtering

Wiener filtering is a simple linear estimation method. It is composed of an inverse kernel and a noise-dependent

- *Z. Zhang is with the Division of Biostatistics, Dalla Lana School of Public Health, University of Toronto. E-mail: jasperz.zhang@mail.utoronto.ca*
- *Z. Zou is with the Department of Computer Science, University of Toronto. E-mail: zhiling.zou@mail.utoronto.ca*

damping factor, as shown in the equations below

$$i_{est} = F^{-1}(\frac{|F(k)|^2}{|F(k)|^2 + 1/SNR(\omega)} \frac{F(b)}{F(k)})$$

where $SNR(\omega)$ is the ratio between the signal variance and noise variance at ω.

3.2 Convolutional Autoencoder

Autoencoder (AE) is an unsupervised neural network-based model which compresses and regenerates data [9]. It is widely used in medical research in high dimensional data reduction and latent feature extraction [10]. In our study, we adapted the network structures of AE by setting the input as noised image and the output as FDCT. AE has two components: An encoder and a Decoder. Equations are shown below:

$$Encoder : Encoded = \sigma_1(W_1 \cdot LDCT) + b_1$$

$$Decoder : Denoised = \sigma_2(W_2 \cdot Encoded) + b_2$$

Convolutional Autoencoder contains convolutional layers which detect spacial information in image data. The structure of the convolutional Autoencoder is shown in Fig. 1. The loss or learning objective of the convolutional Autoencoder is the mean square error (MSE) between denoised LDCT and paired FDCT.

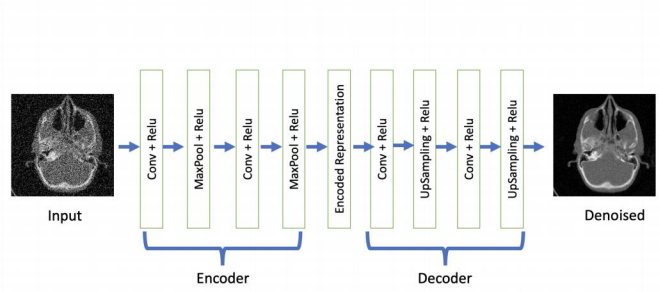

Fig. 1. Convolutional Denoising Autoencoder Network Structure

3.3 DnCNN

Zhang et al. proposed CNN based model DnCNN that learnt the residual distribution, which can handle Gaussian denoising with unknown noise level [11]. AE denoiser is designed to minimize the difference between the denoised image and the FDCT, the truth. Other than AE, DnCNN's learning objective is to find the distribution of noise. All the network layers but the final layer learned the distribution of noise and the final layer substracted predicted noise from the input image and output the denoised image. The network structure of DnCNN is shown in Fig. 2.

3.4 ADMM

The alternating direction method of multipliers (ADMM) is a classical algorithm to solve convex optimization problems [12]. ADMM has low computation time, even when the dataset is large. ADMM decomposes the complex optimization problem into smaller sub-problems. Each sub-problem is then solved using proximal operations. The general form of ADMM is shown in the equation below

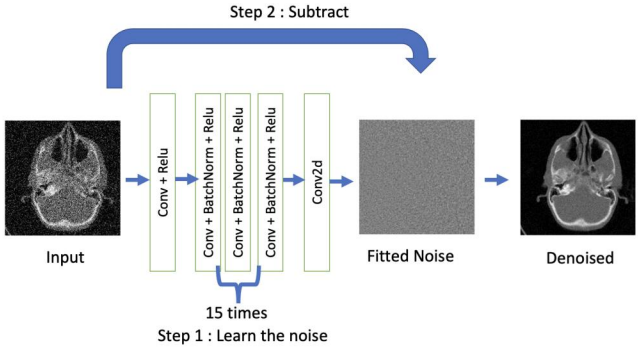

Fig. 2. DnCNN Network Structure

$$\underset{x}{\text{minimize}} \frac{1}{2}\|b - Ax\|_2^2 + \lambda\Gamma(x)$$

where the first term describes the data fidelity and the second term describes some image prior. This equation is subject to $Kx - z = 0$ for some K and z.

3.4.1 TV Prior

The total variation (TV) image prior captures the gradient magnitudes in the image in both X and Y directions. TV prior is suitable for images with sparse gradients, it can be computed as

$$TV(\mathbf{x}) = \|\mathbf{D}\mathbf{x}\|_{2,1} = \sum_{i=1}^{N} \left\| \begin{bmatrix} (\mathbf{D}_x\mathbf{x})_i \\ (\mathbf{D}_y\mathbf{x})_i \end{bmatrix} \right\|_2$$

where $\mathbf{x}$ is the input image.

Hyperparameters used in the TV prior for different types of noises are determined through a parametric sweeping. A set of paired CT scans were used, and the hyperparameters which generate the best denoising performance were selected.

3.4.2 DnCNN Prior

The denoising convolutional neural network (DnCNN) uses a pre-trained DnCNN model as the denoiser. Prior work in [11] [13] was used to characterize the denoiser.

3.5 Experimental Setup

3.5.1 Data Set

The data source is Low Dose CT Image and Projection Data (LDCT-and-Projection-data) from the CPI Cancer Imaging Program from the National Institutes of Health (NIH) [14]. It is a library of CT patient projection data in an open format DICOM-CT-PD. The project has three types of CT scans: head CT, chest CT, and abdomen CT. A subset of 26 patients' head CT was used to evaluate the aforementioned methods. Each patient has 40 paired CT scans, including 20 FDCT and 20 LDCT. The total number of images are 1040. The data set is then split into the training set (80%, 21 patients) and the testing set (20%, 5 patients).

3.5.2 Data Preprocessing

The original square DICOM image size is 512 pixels × 512 pixels. Those images were first down-sampled CT images to 256 pixels × 256 pixels for better computational efficiency.

In addition, artifacts produced by CT machines were presented in some CT images, as shown in Fig. 3 below. As interested anatomical structures are all located in the center of the scans, each CT image was cropped to keep the center region. The cropped images have a size of 200 pixels × 200 pixels. All images are saved to PNG files.

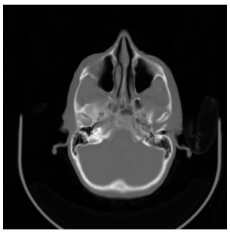

Fig. 3. Example of artifacts on the Edges of N051 CT Image

3.5.3 Additive Noise

To further evaluate the robustness of the denoising methods, simulated noises were applied to the LDCT images. Three noise conditions were considered, Gaussian noise $N(0, \sigma)$ with a standard deviation of 10 noted as $N(0, 10)$, Gaussian noise with a standard deviation of 50 $N(0, 50)$, and Poisson noise $Poi(\lambda)$ with lambda of 50 $Poi(50)$. Generated noisy images are illustrated below in Fig. 4.

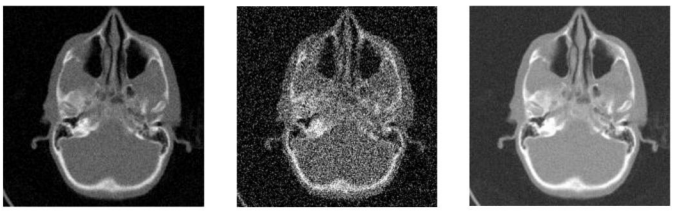

Fig. 4. Simulated Noisy Image of Scan N051 with Different Noise Levels

3.6 Evaluations

The denoising methods described in Section 3 are evaluated both quantitatively and qualitatively.

Two objective image quality metrics are used to measure the performance of the denoising methods. The metrics are computed using the denoised images and the down-sampled full-dose CT (FDCT) images.

Peak signal-to-noise ratio (PSNR) quantifies the ratio between the power of the signal and the power of the noises in the image. A higher value of PSNR often represents a better reconstruction of the noisy image. PSNR is computed using the equation below

$$PSNR(x, y) = \frac{10 \log_{10}[\max(\max(x), \max(y))]^2}{|x - y|^2}$$

Mean Square Error (MSE) quantifies the average pixel difference between the original image and the noisy image. A smaller value of MSE represents a smaller difference. MSE is computed using the equation below

$$MSE = \frac{1}{mn} \sum_{i=1}^{m} \sum_{j=1}^{n} (x_{ij} - y_{ij})^2$$

m	number of rows in cover image
n	number of columns in cover image
x_{ij}	pixel value from cover image
y_{ij}	pixel value from stego image

In addition, the performance of the denoising method will be evaluated based on the perceived image quality in the human eyes.

4 Experimental Results

Denoising methods described in Section 3 were applied to the noisy images sequentially, and the denoised results of one CT scan of patient N051 are demonstrated below in Fig. 5. Zoom in details in the results are demonstrated below in Fig. 6 and Fig. 7.

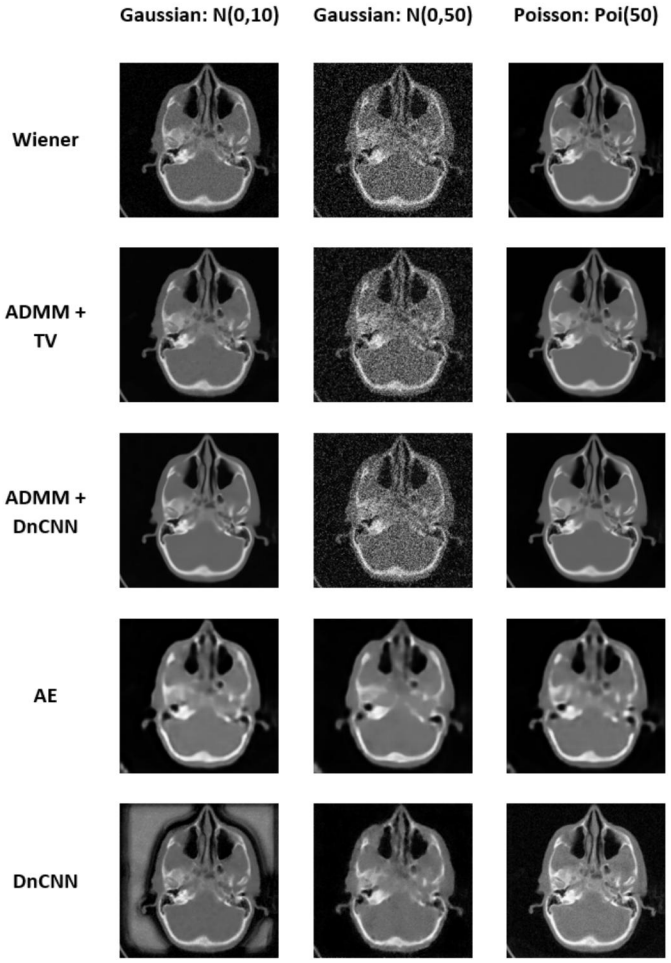

Fig. 5. Denoising Results of one CT Scan of Patient N051 with Different Noise Levels

Through comparing the rows in Fig. 5 qualitatively, it is observed that Wiener filtering has acceptable performance in both $Gau10$ and $Poi50$ noise conditions. However, this

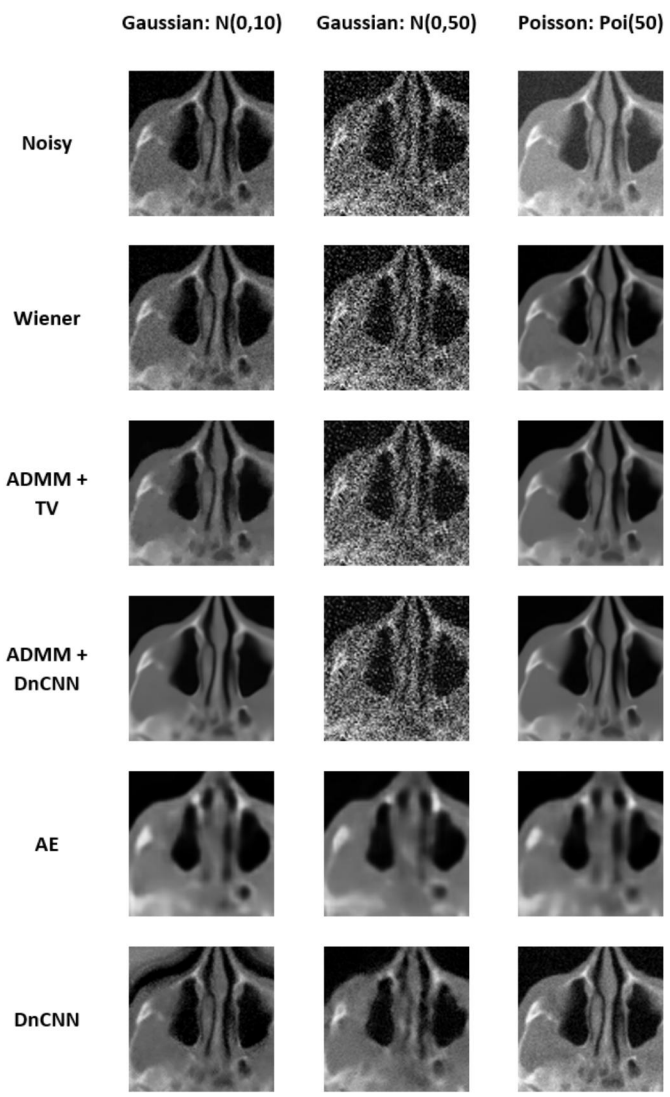

Fig. 6. Zoom in Details in the Denoising Results (Anterior Region) of one CT Scan of Patient N051 with Different Noise Levels

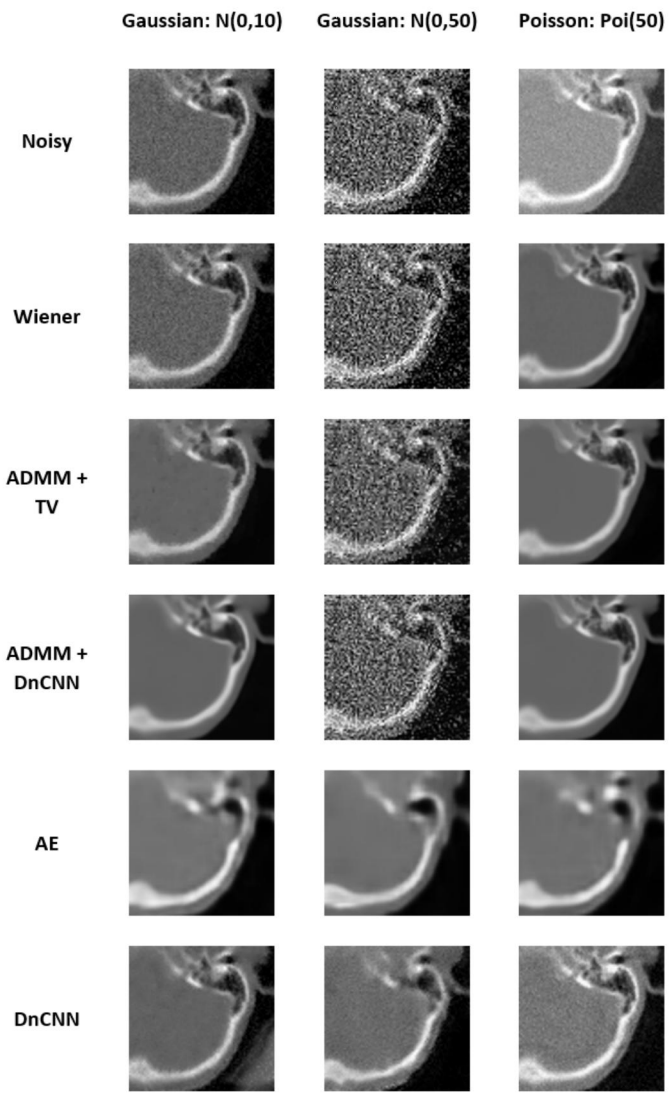

Fig. 7. Zoom in Details in the Denoising Results (Posterior Region) of one CT Scan of Patient N051 with Different Noise Levels

simple filtering method does not perform well in the $Gau50$ noise condition. The Wiener filtering minimizes the overall mean square error regardless of the noise level. It is a linear estimation of the original image. When the simulated noise level is high, or the simulated noise is not simply additive to the image, Wiener filtering is expected not to be effective. Compared to Wiener filtering, two ADMM methods have similar but better performance. They perform well in both $Gau10$ and $POi50$ noise conditions, but they are not very effective in the $Gau50$ noise condition. ADMM solves convex optimization problems. Noise dominates the image in the $Gau50$ noise condition, thus using ADMM-based methods is not ideal. Autoencoder has the most consistent denoising performance along all the methods, noises have been removed for all three noise conditions. DnCNN method has good performance in both $Gau50$ and $Poi50$ noise conditions as well. However, the background in the $Gau10$ noise condition is distorted. DnCNN is designed to learn the distribution of noise if there's a low noise level, there's a chance to overfit the data by considering the background as noise. We can see other than the distorted background, the center of the image shows a good quality of the patient's head slice and provides proper details.

Through comparing the rows in Fig. 6 and Fig. 7 qualitatively, it is observed that ADMM-based methods, especially ADMM with DnCNN, preserved more details than NN-based methods. Results generated by the Autoencoder are blurred, this is especially prominent near the cavities in 6. Autoencoder involves $Maxpool$ and $upsampling$ processes, thus loss of data may be the main reason for this blur. Under $Gau50$ and $Poi50$ noise conditions, the DnCNN method has a good balance between denoising and details preserving, compared to other methods. The residual noises can be visualized in the last picture in Fig. 7. Considering the distorted background of denoised images, the DnCNN is less competitive in quantitative measurements under the $Gau10$ Condition.

The quantitative performance measures of the denoising results are summarized below in Table 1 and Table 2.

Through comparing the results in Table 1, Wiener filtering has the highest PSNR values in both $Gau10$ and $Gau50$ noise conditions, while Autoencoder has the highest PSNR

TABLE 1
PSNR Results of the Denoising Methods and Different Noise Levels

Noise type	Wiener	ADMM+TV	ADMM+DnCNN	Autoencoder	DnCNN
Gaussian: N(0,10)	**47.2**	30.89	29.23	29.79	15.57
Gaussian: N(0,50)	**47.29**	26.05	29.03	28.67	27.75
Poisson: Poi(50)	14.14	14.16	14.18	**29.94**	27.79

TABLE 2
MSE Results of the Denoising Methods and Different Noise Levels

Noise type	Wiener	ADMM+TV	ADMM+DnCNN	Autoencoder	DnCNN
Gaussian: N(0,10)	**0.00002**	0.00082	0.0012	0.00114	0.03034
Gaussian: N(0,50)	**0.00002**	0.00248	0.00125	0.00147	0.0017
Poisson: Poi(50)	0.03858	0.03839	0.03815	**0.00109**	0.00167

values in the $Poi50$ noise condition. ADMM with DnCNN prior performs slightly better on average, compared to ADMM with TV prior. This observation is not consistent to the qualitative comparison discussed above. The reason for this discrepancy is likely due to the fact that the human visual system is nonlinear. Distorted images with additive Gaussian noise, Gaussian blue and high-frequency noise are perceived more prominently in human eyes than the PSNR values.

Similarly, in Table 2, Wiener filtering has the lowest MSE values in both $Gau10$ and $Gau50$ noise conditions, while Autoencoder has the lowest MSE values in the $Poi50$ noise condition. This observation is not consistent with the previous qualitative discussion as well. It is likely due to one limitation of MSE. When an original image is altered by distortion, MSE scores of the distorted images will remain the same. Therefore, MSE is not able to capture blurring and many noises.

5 Conclusion

In conclusion, this work demonstrated satisfying denoising performance on the LDCT head images with the proposed methods. It is found that this denoising could not be simply solved by linear filtering. Autoencoder gives the most consistent denoising performance among the methods. The ADMM-based methods preserve most details in the anatomical structures. Additionally, DnCNN has a balanced performance of denoising and preserving details. PSNR values of the results mostly ranged above 20dB, and MSE values of the results mostly ranged below 0.04.

This project is not without many limitations. First, a relatively small data set was used to train the NN-based methods. More patient data could be included to further increase confidence in the results. Second, only head CT scans are investigated and evaluated. CT scans at different locations will have diverse anatomical structures, Abdomen CT scans and chest CT scans could be included to improve the robustness of the methods. Compared with other large-scale image training tasks, the data size of medical images is relatively small due to the difficulty in collecting data. Pretrained models, such as image GPT, can be an effective first-stage feature learning before training on our CT images [15]. Moreover, more network structures could be studied to explore better options. Popular image processing examples include Diffusion and CycleGAN [16] [17]. Last but not the least, additional features could be developed for this project to expand its use in clinical research, including automatic segmentation and classification of lesions and tumours present in the LDCT scans [18].

The use of LDCT can be accountable in many applications, for example, image-guided therapy and surgeries [19]. There is still much work that needs to be done before the LDCT can be fully adopted in clinical settings. However, it is believed that this work can provide beneficial aid to future work on related topics.

Acknowledgments

We acknowledge Dr. David Lindell and his TA teams Parsa, Shayan, Robin, and Mian for providing us with endless support in learning computational images and designing this project. More importantly, this work is supported by ourselves, with a passion for medical image research.

References

[1] C. Liguori, G. Frauenfelder, C. Massaroni, P. Saccomandi, F. Giurazza, F. Pitocco, R. Marano, and E. Schena, "Emerging clinical applications of computed tomography," *Medical Devices: Evidence and Research*, vol. 8, pp. 265–78, 06 2015.

[2] D. P. Frush, L. F. Donnelly, and N. S. Rosen, "Computed Tomography and Radiation Risks: What Pediatric Health Care Providers Should Know," *Pediatrics*, vol. 112, no. 4, pp. 951–957, Oct. 2003. [Online]. Available: https://doi.org/10.1542/peds.112.4.951

[3] D. Brenner and E. Hall, "Current concepts - computed tomography - an increasing source of radiation exposure," *The New England journal of medicine*, vol. 357, pp. 2277–84, 12 2007.

[4] L. W. Goldman, "Principles of CT: Radiation Dose and Image Quality," *Journal of Nuclear Medicine Technology*, vol. 35, no. 4, pp. 213–225, Dec. 2007, publisher: Society of Nuclear Medicine Section: CONTINUING EDUCATION. [Online]. Available: https://tech.snmjournals.org/content/35/4/213

[5] L. Fan, F. Zhang, H. Fan, and C. Zhang, "Brief review of image denoising techniques," *Visual Computing for Industry, Biomedicine, and Art*, vol. 2, no. 1, p. 7, Jul. 2019. [Online]. Available: https://doi.org/10.1186/s42492-019-0016-7

[6] J. Wang, Y. Guo, Y. Ying, Y. Liu, and Q. Peng, "Fast Non-Local Algorithm for Image Denoising," in *2006 International Conference on Image Processing*, Oct. 2006, pp. 1429–1432, iSSN: 2381-8549.

[7] C. Sutour, C.-A. Deledalle, and J.-F. Aujol, "Adaptive regularization of the nl-means: Application to image and video denoising," *IEEE Transactions on Image Processing*, vol. 23, no. 8, pp. 3506–3521, 2014.

[8] C. Tian, L. Fei, W. Zheng, Y. Xu, W. Zuo, and C.-W. Lin, "Deep Learning on Image Denoising: An overview," Dec. 2019. [Online]. Available: https://arxiv.org/abs/1912.13171v4

[9] I. Goodfellow, Y. Bengio, and A. Courville, *Deep Learning*. MIT Press, 2016, http://www.deeplearningbook.org.

[10] J. Z. Zhang, W. Xu, and P. Hu, "Tightly integrated multiomics-based deep tensor survival model for time-to-event prediction," *Bioinformatics (Oxford, England)*, vol. 38, no. 12, pp. 3259–3266, Jun. 2022.

[11] K. Zhang, W. Zuo, Y. Chen, D. Meng, and L. Zhang, "Beyond a gaussian denoiser: Residual learning of deep cnn for image denoising," *IEEE Transactions on Image Processing*, vol. PP, 08 2016.

[12] S. Boyd, N. Parikh, E. Chu, B. Peleato, and J. Eckstein, "Distributed optimization and statistical learning via the alternating direction method of multipliers," *Foundations and Trends in Machine Learning*, vol. 3, pp. 1–122, 01 2011.

[13] K. Zhang, W. Zuo, and L. Zhang, "Ffdnet: Toward a fast and flexible solution for cnn based image denoising," *IEEE Transactions on Image Processing*, vol. PP, 10 2017.

[14] C. McCollough, B. Chen, D. R. Holmes III, X. Duan, Z. Yu, L. Yu, S. Leng, and J. Fletcher, "Low dose ct image and projection data (ldct-and-projection-data)," The Cancer Imaging Archive, V4, doi: 10.7937/9NPB-2637, 2020.

[15] H. Chen, Y. Wang, T. Guo, C. Xu, Y. Deng, Z. Liu, S. Ma, C. Xu, C. Xu, and W. Gao, "Pre-Trained Image Processing Transformer," in *2021 IEEE/CVF Conference on Computer Vision and Pattern Recognition (CVPR)*. Nashville, TN, USA: IEEE, Jun. 2021, pp. 12 294–12 305. [Online]. Available: https://ieeexplore.ieee.org/document/9577359/

[16] J. Ho, A. Jain, and P. Abbeel, "Denoising Diffusion Probabilistic Models," Dec. 2020, arXiv:2006.11239 [cs, stat]. [Online]. Available: http://arxiv.org/abs/2006.11239

[17] J.-Y. Zhu, T. Park, P. Isola, and A. A. Efros, "Unpaired image-to-image translation using cycle-consistent adversarial networks," in *Computer Vision (ICCV), 2017 IEEE International Conference on*, 2017.

[18] G. Veronesi, P. Maisonneuve, L. Spaggiari, C. Rampinelli, A. Pardolesi, R. Bertolotti, N. Filippi, and M. Bellomi, "Diagnostic performance of low-dose computed tomography screening for lung cancer over five years," *Journal of Thoracic Oncology: Official Publication of the International Association for the Study of Lung Cancer*, vol. 9, no. 7, pp. 935–939, Jul. 2014.

[19] D. Dreizin, A. J. Nam, J. Hirsch, and M. P. Bernstein, "New and emerging patient-centered CT imaging and image-guided treatment paradigms for maxillofacial trauma," *Emergency Radiology*, vol. 25, no. 5, pp. 533–545, Oct. 2018.